

Gas ionization solar spectral monitor (GISSMO)

James S. Vickers¹, Daniel M. Cotton², Timothy A. Cook², and Supriya Chakrabarti²

¹ Space Sciences Laboratory, University of California, Berkeley, CA 94720
and

²Center for Space Physics, Boston University, 725 Commonwealth Avenue, Boston, MA 02215

ABSTRACT

We are currently developing an instrument free from optical components to measure the full-disk solar spectrum in the extreme ultraviolet regime covering wavelengths from 75-400 Å. The instrument consists of a windowless noble gas ionization cell followed by a toroidal electrostatic analyzer to spatially disperse photoelectrons as a function of their energies. A microchannel plate based position sensitive detector is used to detect individual electrons, indirectly returning the solar EUV spectrum. The instrument was launched aboard a NASA Black Brant sounding rocket on October 27, 1992. Power to this instrument was lost early in the flight however, and a reflight is planned for October 1993. Calibration results for the He II 304 Å line are presented.

1. INTRODUCTION

An accurate knowledge of the solar extreme ultraviolet (EUV) flux is central to the fields of geophysics, planetary physics, and interplanetary physics. The solar EUV irradiance, however, is highly variable and remains poorly monitored. Conventional space borne spectrometers capable of measuring the solar irradiance degrade with time, due both to extended instrument exposure to space environment and to the degradation of optical components - typically diffraction gratings and mirrors - which is a result of the solar irradiance itself. In order to accurately measure long term solar irradiances, an instrument is needed which does not suffer such degradations with time.

A standard laboratory technique to measure absolute light intensities involves a photo-ionization chamber^{1, 2}. Inside such a chamber, incoming light photoionizes a suitable gas, producing photoelectrons and ions. By counting the number of electrons and/or ions thus created, a measure of the absolute photon flux is possible. Indeed, this technique is used by the National Institute of Standards and Technology (NIST, formerly the National Bureau of Standards, NBS) for calibrating standard EUV detectors.

Carlson *et al.*³ applied this technique to measure the solar EUV flux in the 50-575Å region during a sounding rocket flight. During this flight, solar EUV photons passed through an aperture into an ionization chamber containing neon, an atomic gas whose cross section for photon⁴ and electron impact⁵ ionization was well studied. The parameters of the ionization chamber, notably the neon pressure and the chamber length, were such that it operated at near total absorption for photons in their wavelength range. An accurate measurement of the integrated solar EUV flux over this wavelength range was made possible by analysis of the measured chamber ion current; spectral information could not be recovered using this technique, however. Samson⁶ addressed this last issue by investigating the use of photoelectron energy distributions to measure the absolute photon spectra.

In this paper we describe the instrument design of GISSMO, a Gas Ionization Solar Spectral MOonitor. GISSMO addresses the need for a spaceborne spectrometer capable of monitoring solar EUV emissions throughout an entire eleven year solar cycle. The instrument combines the advantages of known calibration and long term stability inherent in a gas ionization chamber with a photoelectron energy discriminator to return both the spectral content and the total flux of the ionizing solar radiation. GISSMO was launched aboard a NASA Black Brant sounding rocket (36.098UE) on October 27, 1992. Power to the instrument was lost shortly into the flight however, and no useful data was obtained. The flight has been rescheduled for October 1993, and is primarily intended as a proof of concept.

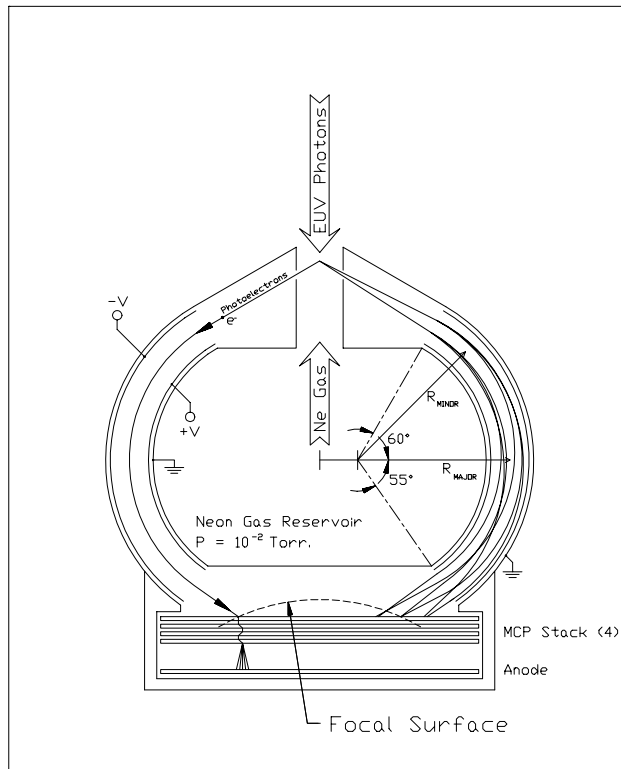


Fig. 1. Schematic diagram of GISSMO.

2. DESIGN OF GISSMO

During gas photoionization, a photon of energy hc/λ is absorbed by a gas atom, producing a photoelectron and an ion. Application of the conservation of momentum principle to this process demonstrates that virtually all of the resulting kinetic energy is carried by the much lighter photoelectron. Consequently,

$$E_e = \frac{hc}{\lambda} - \Phi_i, \quad (1)$$

where E_e and Φ_i represent the electron kinetic energy (after ionization) and gas ionization potential, respectively. Neglecting for now the possibilities of multiple ionization by a single photon and secondary ionizations by photoelectrons, measurement of the energy distribution of photoelectrons from an absorption chamber, coupled with a knowledge of photoabsorption cross-sections and the ionization potential, is seen to return the spectrum of the ionizing radiation. In this manner, spectral information about the sun can be continuously monitored, free from the temporal degradation inherent in conventional optical spectrometers, provided that gas flow through the instrument is maintained and the detector gain remains known.

A schematic illustration of GISSMO is presented in Figure 1, and a photograph appears in Figure 2. For simplicity, a complete cross section is shown, although the instrument is rotationally symmetric to allow collection of electrons over all azimuthal angles. The device consists of a central reservoir, which is maintained at a constant pressure near 1×10^{-2} Torr neon. A tube, aligned in the direction of the sun, vents this gas to space as shown. Solar EUV photons traveling into the reservoir ionize this gas as it is escaping, creating a column source of photoelectrons having energies which depend via Eq. 1 on the solar spectrum. A small fraction of the photoelectrons escapes the tube through circular slits, whereupon they travel through a toroidal electrostatic analyzer. The analyzer is designed to image electrons originating from the slit to a ring on an MCP-based position sensitive detector, with higher energy electrons focusing to larger radius rings. By imaging the location of each photoelectron as it strikes the detector, a

Fig. 2. Photograph of GISSMO. The body of the instrument is 15 cm. in diameter. Seen on the front is the nozzle through which both light enters into and Neon gas escapes from the ionization chamber.

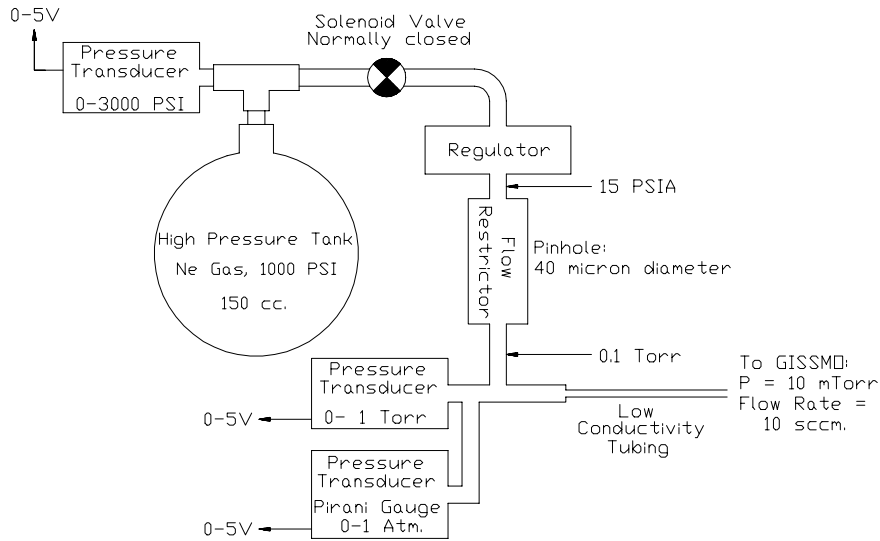


Fig. 3. Schematic diagram of the gas delivery system.

histogram of electron energies is produced, which upon normalization by an energy dependent photoionization cross section, returns the original solar spectrum.

2.1. Gas delivery system

Figure 3 shows a schematic diagram of the gas delivery system responsible for maintaining the pressure in the central reservoir of GISSMO at 1×10^{-2} Torr. A pressure vessel containing 150 cm^3 of neon at 1000 PSI acts as our supply of gas. This volume is sufficient for all test, calibration, and flight activities of the instrument. The gas pressure inside this vessel is monitored by a transducer. Opening an electrically operated solenoid valve connected to this vessel initiates gas flow through GISSMO when the instrument is in space. Once open, a regulator maintains a steady pressure of 15 PSIA on the downstream side. A flow restrictor, consisting of a pinhole approximately $40 \mu\text{m}$ in diameter, is used to restrict neon flow to the 10 std. cm^3/min . rate required by our instrument.

Several options were available when choosing the ionization medium. Although neon is used within our ionization volume, any atomic gas could be used in its place. Molecular gasses, having absorption bands and multiple photoionization mechanisms, are undesirable. Of the atomic gasses, neon offers several advantages over a more likely candidate, helium. Firstly, neon's cross section for photon absorption⁴ can be over an order of magnitude larger than helium's within the wavelength range we will monitor. Secondly, being more massive, neon escapes more slowly from the central gas reservoir, reducing gas consumption. A disadvantage with neon, however, is that photoionization can occur from either the K or L electronic shells. Photons having an energy greater than the K shell ionization potential can conceivably produce two energetically different photoelectrons. Extraction of the true photon spectrum from the measured photoelectron energy spectrum now requires that the two branches be deconvolved.

The signal measured by GISSMO is directly proportional to the density of atoms, and hence the pressure and temperature, within the ionization region. The fundamental uncertainties in solar flux measurements are therefore intimately tied to the pressure and temperature uncertainties within this region. As a result, two low-pressure gauges - a capacitance manometer and a Pirani gauge - fly with GISSMO to provide independent pressure readings. Both gauges have survived the rigorous pre-launch shake tests as well as an actual flight, and can measure the pressure within the ionization region to an accuracy of 0.8%. The temperature of the central gas reservoir is also measured and known to within 0.5°C , or 0.16%. The uncertainty in atomic density is therefore expected to be about 1%.

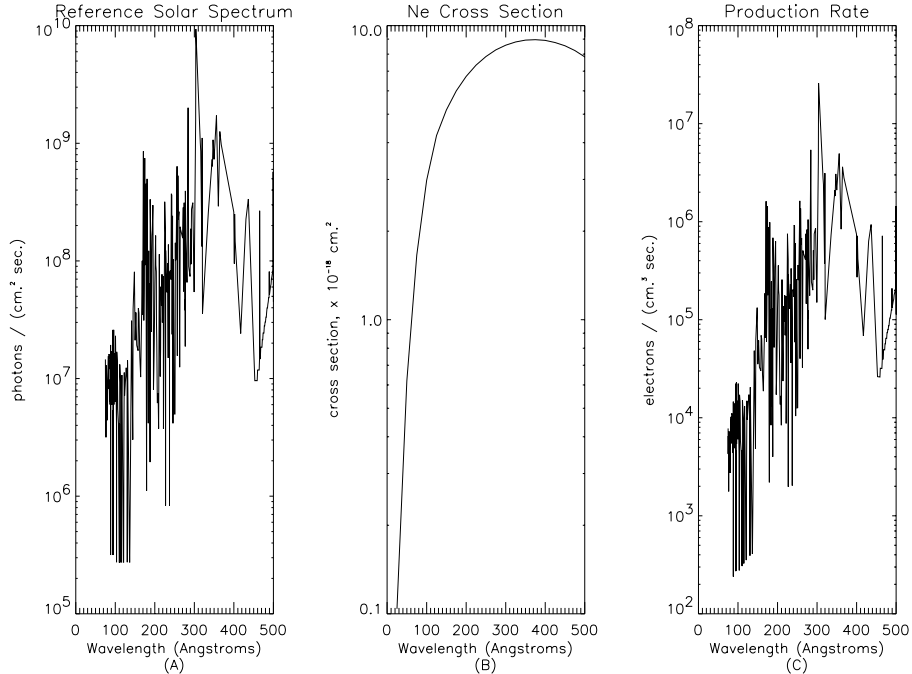


Fig. 4. The reference solar spectrum predicted for September 1992 is shown in Fig. 4a. Fig. 4b shows the photoionization cross section for neon. In Fig. 4c, the photoelectron production rate is shown for the conditions given in Fig. 4a, assuming neon gas at 1×10^{-2} Torr and 300° K.

2.2. Gas ionization region

The gas delivered to the central reservoir vents to space through a tube aligned in the direction of the sun. Solar EUV photons traveling into this region ionize the escaping atoms, creating a column source of photoelectrons. In order to determine the volume production rate of photoelectrons within this region, a solar emission model⁷ was used to predict a solar reference spectrum for our launch date. The data from this model is shown in Figure 4a. Figure 4b shows a plot of the photoionization cross section of neon, using data compiled from Marr *et al.*⁴. The density of neon atoms within the ionization region can be calculated using the measured values of pressure and temperature; for purposes here, a density consistent with a pressure of 1×10^{-2} Torr and a temperature of 300° K is used. This information is combined in Figure 4c, which shows the predicted photoelectron volume production rate as a function of photon wavelength. Note that the production rate varies by three orders of magnitude in the range of wavelengths that GISSMO will observe.

Electrons generated by photoionization of neon have energies given by Eq. 1. However, as these electrons travel through the gas, collisions with other atoms may create additional electrons whose energies differ from that of Eq. 1. In the particular case of GISSMO, a tube diameter of 6.35 mm and a slit height of 2.5 mm is sufficient to provide a maximum count rate of about 10,000 electrons per second on the detector. Using the data of Smith *et al.*⁵ and the atomic neon density used in the preceding paragraph, the mean free path for electron-impact ionization is found to be about 0.4 meter in the shortest case. Because electrons in GISSMO will travel through neon, on average, about 3.2 mm. before escaping through slits, an error of approximately 1% will be introduced as a result of electron impact ionization. A similar calculation shows that roughly 5% of photoelectrons scatter elastically from neutral neon atoms within the ionization region before they escape through the slits into the electrostatic analyzer. Because these collisions are elastic, and because as many electrons are scattered into the slits as are, on average, scattered from the slits, no error in either photon flux or energy is introduced here. Furthermore, the pressure within the electrostatic analyzer is expected to be at least two orders of magnitude less than the pressure within the ionization volume, reducing the error caused by photoelectron scattering within this more critical region. Other aberrations of

Eq. 1, such as those resulting from either multiple ionization of neon^{8, 9} or ionization of multiple atoms by a single photon, are nonexistent for photon energies below the double ionization threshold (63 eV for Ne) and introduce further small and correctable errors at higher energies.

2.3. Electrostatic analyzer

Electrons which escape the ionization region through the slit have energies which depend on the wavelength of the solar radiation responsible for their production. In order to determine the solar spectrum from these electrons, the electron energies must be measured.

Typically, electron energies are measured either with the aid of retarding potentials or with deflecting electric or magnetic fields. In the first case, a retarding electric potential is used to stop all electrons having kinetic energies less than the potential energy of the retarding field. An instrument emphasizing this technique has been developed for flight aboard the CORONAS spacecraft^{10, 11}. In order to determine the electron energy spectrum, a derivative of the number of electrons which overcome this retarding potential with respect to the retarding potential itself must be performed. While this technique is relatively easy to perform and can in principle detect electrons over all solid angles, the required signal differentiation can introduce substantial noise, especially if the signal itself is weak and/or contains noise. The second method uses the deflection of electron trajectories by electric or magnetic fields to precisely measure electron energies of collimated sources. The resolving power of this method generally decreases, however, as the source field of view increases.

Numerous electrostatic analyzer designs have been proposed which offer increased field of view coverage and improved resolution. Paolini *et al.*¹² proposed using the focusing properties of hemispherical plates for an electrostatic analyzer. Using small perturbations from a circular orbit, it can be shown that a $1/r$ potential produces a focusing effect on particles, whereby particles diverging slightly from a point on a circular orbit converge to a point in the orbit 180° opposite. Later, Theodoridis¹³ showed how logarithmic potentials inherent with cylindrical geometries also focus, but require only 127° of orbit. A similar perturbation analysis on these orbits shows that this angle is $90\sqrt{2}^\circ$.

Neither geometry is ideal for our application. Cylindrical geometry can offer only a small field of view coverage. Spherical geometry allows for analysis of particles emitted over all azimuthal angles from a point on one pole of a sphere, but requires electron detection along the radial direction at the other pole.

Toroidal geometries¹⁴, having properties of both spherical and cylindrical geometries, combine many of the advantages of the previous methods. Electrons can be collected over all azimuthal angles and can be focused at some intermediate analyzer angle between 127° and 180° , enabling, with some aberration, imaging using a flat detector. Several geometries were considered before choosing the current design for GISSMO. For each geometry considered, the electrostatic potential Φ due to the analyzer was numerically calculated¹⁵, using relaxation techniques, by solving the Laplace equation in spherical coordinates,

$$\frac{1}{r^2} \frac{\partial}{\partial r} \left(r^2 \frac{\partial \Phi}{\partial r} \right) + \frac{1}{r^2 \sin \theta} \frac{\partial}{\partial \theta} \left(\sin \theta \frac{\partial \Phi}{\partial \theta} \right) = 0. \quad (2)$$

The azimuthal term has been omitted due to the symmetry of the analyzer.

Computer raytraces were then performed to characterize the design. GISSMO uses a toroidal design, with a ratio of R_{major} to R_{minor} (see Fig. 1) of 1.25. The electrostatic analyzer subtends 115° of arc, enough to image photoelectrons from the slit onto rings on the detector. Actual focus by the toroidal analyzer occurs on a curved surface. Optimal placement of the detector was required to minimize distortions caused by mapping this surface onto a flat detector.

Design considerations include the volume in which photoionization occurs and the slit size, which are determined by solar intensities, gas photoionization cross sections and density, and desired detector count rate. Furthermore, the size of the instrument is constrained by the maximum size of the MCPs available for use in the detector.

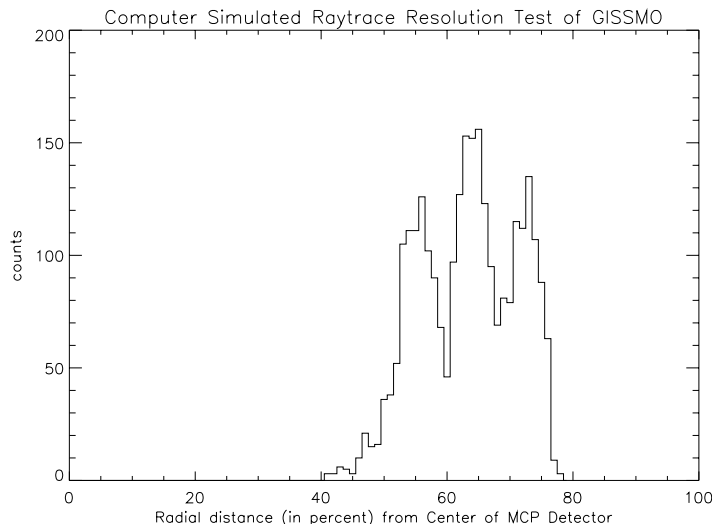


Fig. 5. Raytrace results for three groups of electrons separated in energies by 3% each. The three distinct energy bands are clearly resolved, yielding a resolution of 33.

Analyzer resolution is reduced when either the ionization area or slit size is increased, or when desired field of view coverage is increased, requiring a tradeoff between sensitivity and resolution. GISSMO has been designed to operate with a resolution R of 33, defined as $R \equiv \frac{\lambda}{\Delta\lambda}$, although higher resolutions can easily be realized with this type of analyzer. Because this rocket flight represents a proof of concept for GISSMO, and due to the short duration of the flight, resolution has been partially sacrificed in order to increase sensitivity.

Data from the raytrace program is shown in Figure 5. Photoelectrons originating at random locations from within the ionization region were traced through the instrument. Of those that made it through both the slit and analyzer, their radial position as they struck the detector was recorded. This process was recorded for three sets of photoelectrons separated in energy by $1/R$, or 3%. The energies are clearly resolved. Bandpass measurements were also made, showing that approximately six such 3% bands make it through GISSMO, all resolved.

In practice, stray magnetic fields within the electrostatic analyzer limit the resolution for low energy photoelectrons. The photoelectron gyro radius, r_e , is given in SI units by

$$r_e = \sqrt{\frac{2m_e V}{eB^2}} \quad (3)$$

where m_e , e , and V are the electron mass, charge, and potential respectively, and B is the magnetic field. Using for B the earth's magnetic field, $r_e \approx 6.7\sqrt{V(\text{in volts})}$ cm. This radius is to be compared with the radius of curvature of the electrostatic analyzer, which is approximately 4 cm. As a result, photons with energies slightly above the ionization threshold of Ne (ie. having low potential V) will be mis-analyzed by GISSMO. To minimize this problem, critical items in GISSMO were fabricated using mumetal to shield the electrostatic analyzer from magnetic fields. Still, the measured resolution fell below our goal of $R = 33$ for photons having wavelengths between approximately 400\AA and 575\AA , the ionization threshold of neon. This problem could easily be remedied for a long duration space mission by fabricating a smaller, lighter, and better shielded GISSMO.

GISSMO will cover the spectral range of $75\text{-}400\text{\AA}$ by adjusting the voltage, $+V$ and $-V$ shown in Fig. 1, on the electrostatic analyzer. Different spectral bands can therefore be selected electronically, and do not require mechanical scanning techniques. Separate gas ionization techniques have been used at wavelengths of 20\AA ¹⁶ and below. Although GISSMO will only monitor down to 75\AA , the design is capable of observing photons of shorter

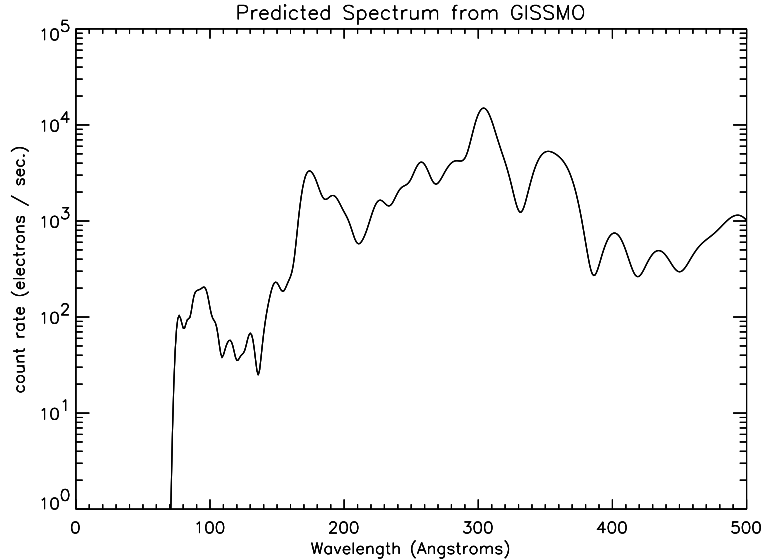


Fig. 6. Predicted electron count rate for GISSMO assuming 1×10^{-2} Torr neon, 300° K., and a resolution $R = 33$.

wavelength. Below 75 \AA , a combination of decreasing photoionization cross sections and diminishing solar output necessitates longer scanning times. The wavelength cutoff of 75 \AA was chosen to allow enough time during the rocket flight to perform several complete spectral scans.

2.4. Detector

GISSMO employs a MCP imaging detector to count individual photoelectrons. The MCPs have an active diameter of 74 mm, with a $25 \mu\text{m}$ pore diameter and a 40-1 aspect ratio. Because of the worry that excess neon atoms could make their way into the detector and produce significant ion feedback, four MCPs are used, rather than the three typically used, for electron amplification. With less gain required of each plate, and by orienting the plates in W-stack configuration, the chance of ion feedback occurring within the MCP pores is reduced. A standard wedge, strip, and zig anode¹⁷ is used to find the centroid of the charge cloud produced by the MCP stack. Although Siegmund *et al.*¹⁸ have achieved a resolution greater than 600×600 pixels using a 50 mm imaging detector, GISSMO will operate with only 256×256 pixel resolution, of which only a small fraction are actually needed to resolve the expected eight distinct energy rings on the detector. The central region of the detector is not exposed to photoelectrons, enabling a simultaneous dark count rate measurement to correct for the signal.

The electrostatic analyzer has been designed so that photoelectrons entering the detector region must see a ground potential. This necessitates that the top of the MCP stack (See Fig. 1) be held at ground and that the anode be held at high positive potential. AC-coupling capacitors pass charge deposited at high potential on the anodes to standard charge amplifiers which expect virtual ground anode inputs.

3. INSTRUMENT PERFORMANCE

The reference solar spectrum can be combined with neon photoionization cross section data, the expected instrument resolution of 33, the effective ionization area, the slit size, and the expected density of neon atoms within the ionization region to predict the electron count rate for GISSMO. This information is presented in Figure 6.

The predicted count rate for wavelengths in the $75\text{-}400 \text{ \AA}$ range is seen to vary by three orders of magnitude. Although this dynamic range is easily accommodated by the GISSMO design, further reduction of the lower wavelength limit would require additional dynamic range. This too presents few problems as, for instance, a second valve

could be opened to increase neon concentration within the ionization region during low wavelength measurements.

The electron optics and detector was first tested using 100 eV electrons generated by a hot filament source placed within the ionization region of GISSMO. With voltages of ± 24 V on the electron analyzer plates, 6 clear rings of electrons were imaged onto the detector as the electron energy was changed in two volt increments from 90 to 100 eV. This data suggests that at these relatively high energies, analyzer resolution $R \approx 50$.

GISSMO was calibrated using the He II 304 Å emission line from a gas discharge source. Figure 7 shows data from three separate calibration runs. In each case, the He II 304 Å flux was approximately 5×10^7 photons/sec./cm.². Since the solar flux at this wavelength is approximately 200 times greater than our calibration flux, we expect a two hundred fold increase in the signal to noise ratio during flight.

The resolution of GISSMO can be estimated using Figures 7a, 7b, and 7c. Because the photoelectrons energy could not be changed in this test, the electron analyzer plate potential was varied instead, from ± 4.5 V in Figure 7a, ± 4.7 V in 7b, to ± 4.9 V in 7c. When superimposed, the three rings are resolved, demonstrating that the resolution, R , of GISSMO at these wavelengths is in excess of 25.

4. CONCLUSION

GISSMO was launched aboard a Black Brant sounding rocket (36.098UE) on October 27, 1992. Unfortunately, power to this instrument was lost early in the flight and no useful data was received. A reflight is scheduled for October 1993. GISSMO will monitor solar EUV emissions in the wavelength range from 75-400Å. The instrument consists of a windowless ionization chamber filled with low pressure neon gas. A toroidal electrostatic analyzer focuses photoelectrons leaving this chamber in a 360° azimuthal by 8° polar solid angle onto a MCP-based detector. Different energy bands are individually focused to separate radius rings on the detector. We expect a resolving power, defined as $\lambda/\Delta\lambda$, of about 33. Because instrument operation is based on an ionization chamber rather than on conventional optics, absolute calibration is possible for as long as gas flow is maintained. We believe that GISSMO addresses the need for a satellite-based monitor of solar EUV emissions which is capable of maintaining calibration over a significant portion of the eleven year solar cycle.

5. ACKNOWLEDGEMENTS

The authors would like to express their gratitude to Don Zukauckas and Chris Scholz for their technical assistance in assembling GISSMO electronics. Many thanks are also due to Dean Colomb and Terry McDonald for the craftsmanship displayed in building GISSMO. We thank Igor Rebo for getting us started on this path of photoionization spectroscopy, and acknowledge many useful discussions with Justin Bendich, Charles Carlson, James McFadden, Michael Gruntman, Darrell Judge, Howard Ogawa, and James Samson. This work has been supported by NASA grant NAG5-680.

6. REFERENCES

1. James A. R. Samson, "Absolute Intensity Measurements in the Vacuum Ultraviolet," *J. Opt. Soc. Am.*, 34, pp. 6-15, 1964.
2. T. Sasaki, T. Oda, and H. Sugawara, "Measurement of Absolute Intensity of Radiation in XUV by a Rare-Gas Photoelectron Counter," *Appl. Optics* 16, pp. 3115-3121, 1977.
3. Robert W. Carlson, H. S. Ogawa, E. Phillips, and D. L. Judge, "Absolute Measurement of the Extreme UV Solar Flux," *Appl. Optics* 23, pp. 2327-2332, 1984.
4. G. V. Marr and J. B. West, "Absolute Photoionization Cross-Section Tables for Helium, Neon, Argon, and Krypton in the VUV Spectral Regions," *At. Data Nucl. Data Tables* 18, pp. 497-508, 1976.
5. P. T. Smith, "The Ionization of Helium, Neon, and Argon by Electron Impact," *Phys. Rev.* 36, 1293, 1930.
6. J. A. R. Samson, "Vacuum Ultraviolet Radiometry and Wavelength Standards," International Symposium for Synchrotron Radiation Users, Daresbury, Jan. 4-7 1973.

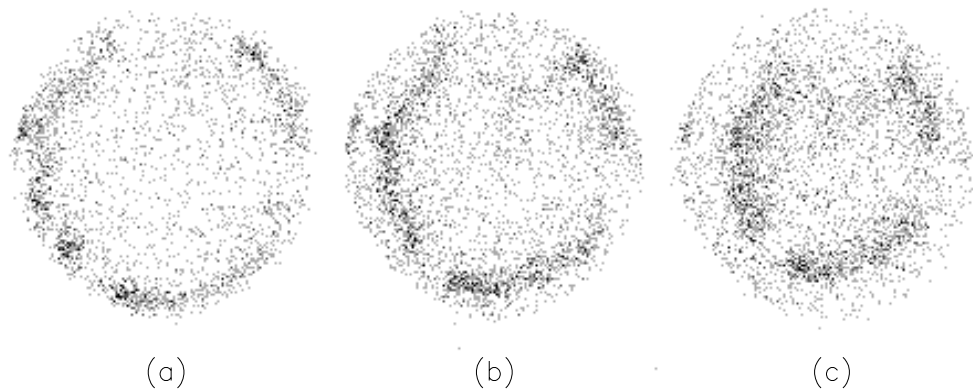


Fig. 7. GISSMO calibration results using He II 304 Å light from a gas discharge source. The He II 304 Å flux was 5×10^7 photons/sec./cm.², approximately 200 times less than the expected solar flux at this wavelength. The electron analyzer plate potential was: a) ± 4.5 V, b) ± 4.7 V, and c) ± 4.9 V.

7. K. Tobiska, "Revised Solar Extreme Ultraviolet Flux Model," *J. Atmos. and Terr. Phys.* 53, 1005, 1991.
8. James A. R. Samson and G. N. Haddad, *In Electron and Photon Interactions with Atoms*, Edited by H. Kleinpoppen and M. R. C. McDowell, pp. 133-139, Plenum Publishing Corp., New York, 1976.
9. T. A. Carlson, "Double Electron Ejection Resulting from Photo-Ionization in the Outermost Shell of He, Ne, and Ar, and its Relationship to Electron Correlation," *Phys. Rev.* 156, 142, 1967.
10. E. D. Mishchenko and I. L. Rebo, "Improvement in the Threshold Sensitivity of a Photoionization Colliding Spectrometer," *Opt. Spectrosc.* 62, 261, 1987.
11. E. D. Mishchenko, I. L. Rebo, and A. B. Utkin, "The Effects of Magnetic Field Inhomogeneities on the Operation of a Collisional Spectrometer," *Opt. Spectrosc.* 62, 703, 1987.
12. F. R. Paolini and G. C. Theodoridis, "Charged Particle Transmission Through Spherical Plate Electrostatic Analyzers," *Rev. Sci. Instrum.* 38, pp. 579-588, 1967.
13. G. C. Theodoridis and F. R. Paolini, "Charged Particle Transmission Through Cylindrical Plate Electrostatic Analyzers," *Rev. Sci. Instrum.* 39, pp. 326-330, 1968.
14. D. T. Young, S. J. Bame, M. F. Thomsen, R. H. Martin, J. L. Burch, J. A. Marshall, and B. Reinhard, "2 π -Radian Field of View Toroidal Electrostatic Analyzer," *Rev. Sci. Instrum.* 59, pp. 743-751, 1988.
15. M. J. Sablik, D. Golimowski, J. R. Sharber, and J. D. Winningham, "Computer Simulation of a 360° Field of View 'Top-Hat' Electrostatic Analyzer," *Rev. Sci. Instrum.* 59, pp. 146-155, 1988.
16. W. Feng, H. S. Ogawa, and D. L. Judge, "The Absolute Solar Soft X-Ray Flux in the 20- to 100-Å Region," *J. Geophys. Res.* 94, pp. 9125-9130, 1989.
17. C. Martin, P. Jelinsky, M. Lampton, R. F. Malina, and H. O. Anger, "Wedge and Strip Anodes for Centroid-Finding Position Sensitive Detectors," *Rev. Sci. Instrum.* 52, 1967, 1981.
18. O. H. W. Siegmund, M. Lampton, J. Bixler, S. Chakrabarti, J. Vallergera, S. Bowyer, and R. F. Malina, "Wedge and Strip Image Readout System for Photon-Counting Detectors in Space Astronomy," *J. Opt. Soc. Am. A* 3, 2139, 1986.